Photoswitches

International Edition: DOI: 10.1002/anie.201710443
German Edition: DOI: 10.1002/ange.201710443

Nanoscale Chemical Imaging of Reversible Photoisomerization of an Azobenzene-Thiol Self-Assembled Monolayer by Tip-Enhanced Raman Spectroscopy

*Li-Qing Zheng, Xing Wang, Feng Shao, Martin Hegner, and Renato Zenobi**

Abstract: *An understanding of the photoisomerization mechanism of molecules bound to a metal surface at the molecular scale is required for designing photoswitches at surfaces. It has remained a challenge to correlate the surface structure and isomerization of photoswitches at ambient conditions. Herein, the photoisomerization of a self-assembled monolayer of azobenzene-thiol molecules on a Au surface was investigated using scanning tunneling microscopy and tip-enhanced Raman spectroscopy. The unique signature of the cis isomer at 1525 cm^{-1} observed in tip-enhanced Raman spectra was clearly distinct from the trans isomer. Furthermore, tip-enhanced Raman images of azobenzene thiols after ultraviolet and blue light irradiation are shown with nanoscale spatial resolution, demonstrating a reversible conformational change. Interestingly, the cis isomers of azobenzene-thiol molecules were preferentially observed at Au grain edges, which is confirmed by density functional theory.*

Molecular switches, which undergo molecular-scale motion upon external stimuli, are very promising for molecular electronics and high-density data storage. However, a deeper understanding of their mechanical and electronic properties at the molecular level is required for developing applications in the areas of information processing, energy, and biology.[1–4] Of the various molecular switches studied, azobenzene and its derivatives adsorbed on surfaces, one of the most thoroughly investigated classes of molecular switches,[5–7] have attracted considerable attention in the last few years thanks to their practical applications as nanomotors,[8] in adaptive imaging,[9] and as energy storage devices[10] when binding to adaptive surfaces. The photoisomerization of azobenzene can be triggered by illumination at the appropriate wavelength. Azobenzene undergoes *trans*-to-*cis* isomerization when irradiated with ultraviolet (UV) light (365 nm). The conformational change can be reversed by blue light (450 nm), but it can also be caused thermally in the dark owing to the greater thermodynamic stability of the *trans* isomer.[6,11–13] Moreover, the isomerization can be induced mechanically,[14] thermally,[15] and electrostatically.[16]

Photoisomerization of different molecular switches, for example 3,3′,5,5′-tetra-tert-butyl-azobenzene (TBA),[17] 3,5-di-tert-butyl-N-(3,5-di-tertbutylbenzylidene) aniline (TBI),[18] or azobenzene thiol (ABT),[19] adsorbed on an Au(111) surface has already been demonstrated. The mechanism governing the isomerization behavior of azobenzenes in solution, which is based on n–π*[20,21] or π–π*[22] electronic transitions, is well understood from ultrafast time-resolved studies such as coherent resonant Raman scattering.[23–25] However, the mechanism of the photoisomerization of azobenzenes is quite different when they are in direct contact with a metal surface, in contrast to the photoswitching in solution. The observation that azobenzene fails to isomerize on Au(100) or Cu(111) shows a strong substrate dependence.[26] To date, questions about the switching mechanism of surface-bound molecules under ambient conditions remain.

For a complete understanding of the isomerization processes of ABT on a Au surface, it is important to provide information on both the surface structure and the molecular fingerprint with nanometer spatial resolution, so that the relationship between structure and chemical behavior can be established.[27–29] Tip-enhanced Raman spectroscopy (TERS) is a near-field optical technique that combines the advantages of scanning probe microscopy (SPM) and plasmon-enhanced Raman spectroscopy.[30–34] In this method, an electrochemically etched Ag or Au tip amplifying the electromagnetic field of incident laser light enhances the Raman signal of sample molecules located close to the tip. TERS possesses high spatial resolution and high sensitivity, down to the single molecule level.[28,35] TERS is ideally suited to study defects and step edges, which may play a significant role in surface reactions.[36] Only very few studies have so far addressed the photoswitching properties of metal-surface-bound ABT at ambient conditions, under which molecular switches are used in practical applications.[2,37] The photoisomerization of ABT and an ABT derivative has been probed by surface-enhanced Raman spectroscopy[12] and scanning tunneling microscopy (STM)[37] at ambient conditions, respectively. The reversibility[12] and a cooperative mechanism[37] of the photoisomerization were shown.

Herein, we report the investigation of the isomerization mechanism of an ABT self-assembled monolayer (SAM) on a template-stripped (TS) Au surface[38] (Supporting Information, Figure S1) using ambient STM-TERS, taking advantage of the strong scattering properties of ABT. The reversible photoisomerization behavior of an ABT SAM on a Au surface was demonstrated, based on the presence or absence

[*] L.-Q. Zheng, X. Wang, F. Shao, Prof. Dr. R. Zenobi
Department of Chemistry and Applied Biosciences, Swiss Federal Institute of Technology, ETH Zurich
8093 Zurich (Switzerland)
E-mail: renato.zenobi@org.chem.ethz.ch
Prof. Dr. M. Hegner
Center for Research on Adaptive Nanostructures and Nanodevices, School of Physics, Trinity College Dublin
Dublin 2 (Ireland)
Supporting information and the ORCID identification number(s) for the author(s) of this article can be found under: https://doi.org/10.1002/anie.201710443.

of the characteristic vibrational mode at 1525 cm^{-1} of the *cis* isomer after UV irradiation (ex situ). Furthermore, TERS maps were used to monitor the isomerization of ABT, and to obtain the local information of the reactivity. Interestingly, the *cis* isomers of ABT molecules were preferentially observed at the grain edges of Au. This is ascribed to the lower reaction energy of *trans*-to-*cis* isomerization at Au steps owing to the shift of d bands and different molecular orientation. These results underline that grain edges play a significant role in the photoswitching behavior of surface-bound molecules.

TER spectra of the ABT SAM before and after UV irradiation for 5 min are shown in Figure 1 A. One can see new peaks appearing at 1525 cm^{-1} and 1107 cm^{-1} (weak band) after the sample was irradiated with 365 nm light. The peaks at 1525 cm^{-1} and 1107 cm^{-1} correspond to the υ_{sym}(N=N) mode, and the C–N stretching/ring breathing modes of the *cis* isomer, respectively. Their presence clearly indicates that *trans*-to-*cis* isomerization of ABT occurred. To gain further insight into the Raman peaks observed in the TER spectra and their correlation with the *trans-cis* photoisomerization of azobenzene thiol molecules, B3LYP/6-31G* calculations[12] of the Raman spectra of the *trans* and *cis* isomers of ABT were performed. The dependence of the spectrum on the mole fractions of the two isomers is shown in Figure 1 B. The

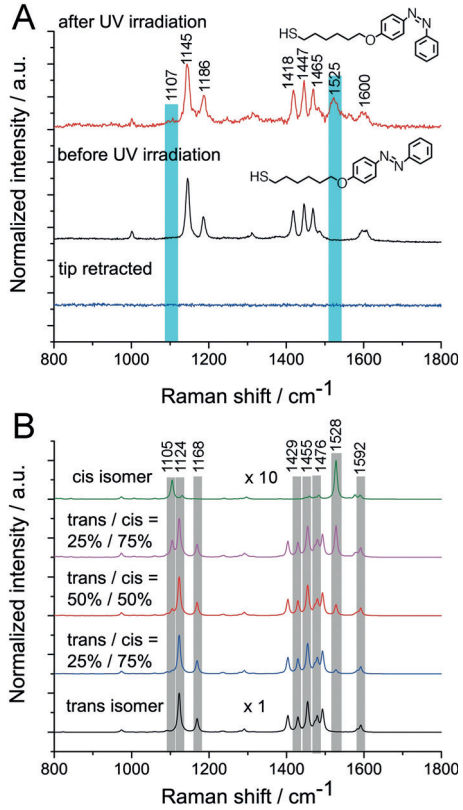

Figure 1. A) TER spectra of an ABT SAM before and after ex-situ UV irradiation for 5 min, as well as a spectrum with the tip retracted. The blue bars indicate the Raman peak at 1525 cm^{-1} and 1107 cm^{-1}, which are characteristic for the *cis* isomer. B) Simulated Raman spectra of the *trans* and *cis* isomers of ABT with different mole fractions of the two isomers.

calculated frequencies were multiplied by a scaling factor of 0.97 to correct for the anharmonicity.[39] The *cis* spectrum is an order of magnitude weaker than the *trans* spectrum. The intensity decrease of the *cis* spectrum may be due to the loss of conjugation of the *cis* isomer and the consequent reduced polarizability and Raman intensity.[12] To compensate for this intensity difference, the intensity of the *cis* isomer's spectrum was magnified 10-fold. To have a better view of the modes, all the Raman peaks were normalized to the most intense Raman peak in each spectrum. We assigned the Raman peaks of ABT according to the calculated spectra (see the Supporting Information, Figure S2). The peaks at 1145 cm^{-1} and 1186 cm^{-1} are skeletal modes with C–N stretching and ring breathing components. The band at 1418 cm^{-1} corresponds to the in-plane ring bending mode with a minor contribution from the N=N stretching mode of the *trans* isomer. The Raman peak at 1447 cm^{-1} is the H–C–H bending mode of the alkyl group. The peak at 1465 cm^{-1} is predominately an N=N stretching mode of the *trans* isomer with minor contributions from the in-plane ring bending mode of the benzene group and the H–C–H bending mode of the alkyl group. The band at 1600 cm^{-1} is a C=C stretching mode.[40,12] Upon *trans*-to-*cis* isomerization of ABT, the υ_{sym}(N=N) frequency shifts from 1465 cm^{-1} to 1525 cm^{-1}, while, the C–N stretching/ring breathing mode shifts from 1145 cm^{-1} to 1107 cm^{-1}. Since the most intense Raman peak of the *cis* isomer is at 1525 cm^{-1}, it can be used as a reporter peak. After UV irradiation, all of the peak intensity ratios between the *trans* peaks and the 1600 cm^{-1} band belonging to both the *trans* and *cis* isomers of the ABT SAM decrease (Supporting Information, Table S1), which also indicates the *trans*-to-*cis* isomerization of ABT. Based on the simulated spectra for different molar ratios of the two isomers, the TER spectrum of the ABT SAM after UV irradiation shown in Figure 1 A is in good agreement with a *trans*/*cis* molar ratio equal to 1:1 (see the Supporting Information, Figure S3). The low intensity of the peak at 1107 cm^{-1} could be due to TERS surface selection rules.[35]

The photoisomerization behavior of an ABT SAM on a semi-transparent Au surface was first verified using UV/Vis spectroscopy. The absorbance difference at 340 nm of the ABT SAM before and after UV irradiation is shown in the Supporting Information, Table S2. The absorbance at 340 nm decreases upon irradiation by UV light, confirming that *trans*-to-*cis* photoisomerization on the Au surface takes place. Moreover, when the irradiation time is prolonged from 5 min to 15 min, the value remains the same. This indicates that the steady-state *trans*-to-*cis* isomerization yield of the ABT SAM is already reached after a UV irradiation time of 5 min. Upon irradiation with blue light for 15 min, the absorbance at 340 nm recovers, indicating *cis*-to-*trans* isomerization.

The lifetime of the *cis* isomers on a Au surface is of great importance. The absorbance change at 340 nm of an ABT SAM on a Au surface after UV irradiation as a function of time is shown in the Supporting Information, Figure S4. The plot was fitted to an exponential function. The thermal back-reaction on the surface is dominated by first-order kinetics with a reaction rate constant of 5.67×10^{-5} s^{-1}. The lifetime of the *cis* isomer on the Au surface is thus around 5 h, which is sufficient for the acquisition of a TERS map. Isomerization of

ABT in ethanol solution is shown in the Supporting Information, Figure S5.

TERS maps of an ABT SAM on a TS Au surface before and after irradiation of UV light were collected. Since the characteristic peak of the *cis* isomer is at 1525 cm^{-1}, which is in the region where spurious peaks from carbonaceous decomposition products usually appear, a very low laser power and a short exposure time were used to collect the TERS maps. Figure 2 shows the TERS peak intensity ratio

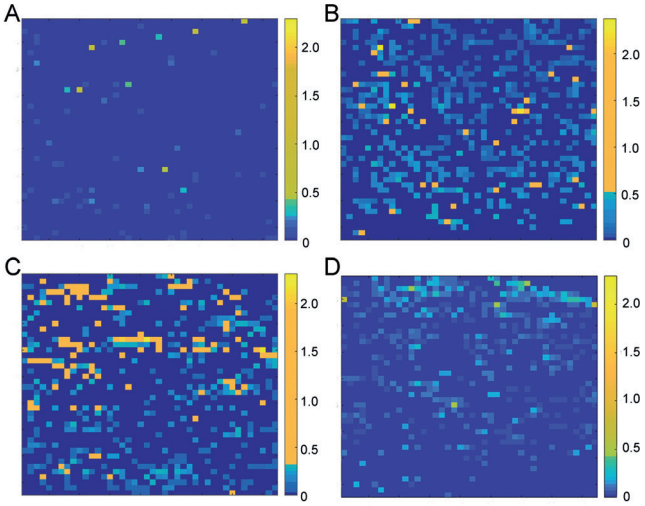

Figure 2. TERS peak intensity ratio (1525 cm^{-1} peak/1143 cm^{-1} peak) maps of ABT SAM A) before and after UV irradiation for B) 5 min and C) 15 min. The sample was prepared in the following way: ABT molecules were first self-assembled on a TS Au substrate, followed by irradiation with UV light for 5 min and 15 min. D) TERS peak intensity ratio map of the ABT SAM after UV irradiation. Sample preparation: ABT in ethanol was first irradiated with UV light for 5 min and then deposited onto a TS Au substrate. The size of the maps is 200×200 nm^2 with a 4.8 nm pixel size. The acquisition time for each spectrum was 1 s.

(1525 cm^{-1} peak/1143 cm^{-1} peak) maps of the ABT SAM on the Au surface before and after UV irradiation for different times. A dark blue color corresponding to 0 in the scale bar indicates that there is no Raman peak at 1525 cm^{-1} in that particular region. In Figure 2A, we can barely see the *cis* peak. After the ABT SAM was irradiated with UV light for 5 min, the Raman peak at 1525 cm^{-1} appeared much more frequently than before, indicating that a fraction of the ABT molecules underwent a *trans*-to-*cis* isomerization (Figure 2B). This peak is irregularly distributed and present in 29% of all the pixels. To assess the variability of the peak at 1525 cm^{-1} associated with the isomerization of ABT, principal component analysis (PCA) on Figure 2B was performed. PC1 corresponds to the TER spectrum of *trans* isomer, while PC2 may correspond to that of *trans* and *cis* isomers (Supporting Information, Section S3). Only a very small contribution from PC3, which stems from carbon contamination, is present in the spectra. This suggests that sample decomposition is minor.

When the exposure time was increased to 15 min, the presence of the Raman peak at 1525 cm^{-1} in the whole map was slightly decreased to 26%, which is a bit surprising. We interpret this to be due to the thermal back-reaction during the TERS mapping (Figure 2C). From the data in Figure 2C, the spatial resolution was estimated to be around 10 nm based on a full-width at half-maximum (FWHM) analysis (Supporting Information, Figure S8).

Another sample preparation method was tested to check the different isomerization rate of ABT in ethanol solution and as a SAM on the Au surface. ABT in ethanol solution was first irradiated with UV light for 5 min and then deposited onto a Au surface, which takes circa 120 min. Finally, the TERS map of the ABT SAM sample was collected (Figure 2D). The proportion of the *cis* peak in the whole map is 23%, which is smaller than that in Figure 2B. This indicates that a fraction of the ABT molecules present as *cis* isomers must have reacted back to the *trans* isomers, while assembly on the Au surface was carried out. When ABT molecules are bound to a metal surface, the lifetime of the *cis* isomers decreases.

The ABT SAM on the Au surface was irradiated with UV light for 5 min and then irradiated with blue light for 5 min. The TERS map and the corresponding STM image are shown in Figure 3. The fraction of pixels showing the *cis* peak in the

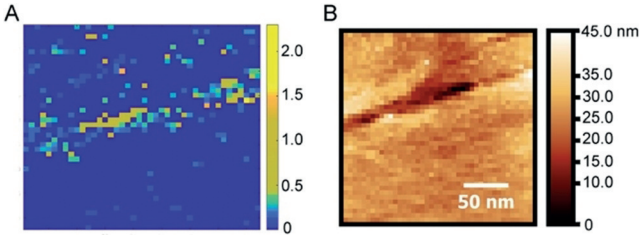

Figure 3. A) TERS peak intensity ratio (1525 cm^{-1} peak/1143 cm^{-1} peak) map of an ABT SAM after UV irradiation for 5 min followed by blue light irradiation for 5 min. B) STM image of ABT SAM on the Au surface acquired together with the TERS map. The size of the map is 200×200 nm^2 with a 4.8 nm pixel size. The acquisition time for each spectrum was 1 s.

whole map is 14%, much smaller than that in Figure 2B and Figure 2C. This indicates that most of the *cis*-ABT molecules had isomerized back to the *trans* form. However, we clearly observe a ribbon of *cis* ABT located in the middle of the map, making up 72% of all pixels containing the *cis* peak. Interestingly, when comparing the topography collected simultaneously with the TERS map (Figure 3B), we found that this *cis* ribbon is situated at a place where there is a Au grain edge. Moreover, the TERS peak intensity ratio (1418 cm^{-1}/1600 cm^{-1}) map is complementary to the TERS peak intensity ratio (1525 cm^{-1}/1600 cm^{-1}) map (Supporting Information, Figure S9). Two further peak ratio maps of ABT adsorbed at terraces and grain edges of Au before UV illumination are shown in the Supporting Information, Figures S10 and S11. One can barely see any peak from the *cis* isomer. Moreover, there is no obvious decrease of the (1418 cm^{-1}/1600 cm^{-1}) peak intensity ratio in the region where there is a Au grain edge (Figures S10B,C and S11B,C), which indicates that the complementary peak intensity ratio maps shown in Figure S9 are not induced by

different orientations of molecules adsorbed on grain edges. Therefore, the results shown in Figure S9 clearly suggest that the *cis*-to-*trans* isomerization at the grain edge of Au is slower than that on the terrace.

To confirm that the isomerization behavior at grain edges of Au is different from that on terraces, several high-resolution TERS measurements going across a terrace and a grain edge on Au were performed, and the results are shown in Figure 4 and the Supporting Information, Figures S12 and

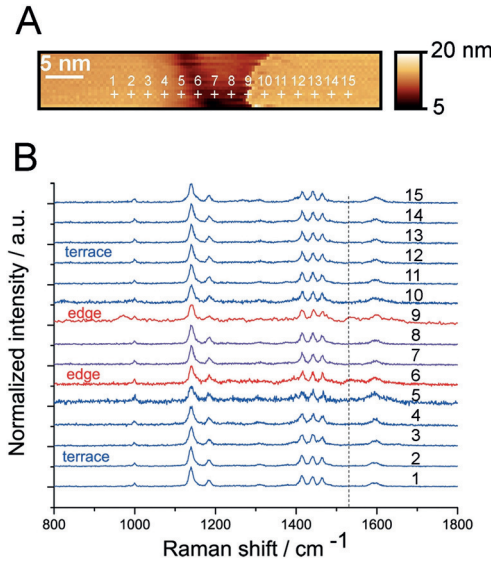

Figure 4. A) STM image of the Au surface covered with an ABT SAM after UV irradiation for 5 min, obtained using an Ag tip. B) Line-trace TER spectra along the crosses indicated in (A). One spectrum was acquired every 2 nm. The exposure time per spectrum was 1 s.

S13. We observed that the peak at 1525 cm^{-1} has a strong preference to be observed at Au grain edges (Figure 4B and Figures S12B and S13B). Moreover, all of the peak intensity ratios between *trans* peaks and the 1600 cm^{-1} peak in the TER spectra of ABT adsorbed at the Au grain edges after UV irradiation (shown in Figure 4B) are smaller than that of ABT adsorbed on Au terraces (Supporting Information, Figure S14), which also indicates that *trans*-to-*cis* isomerization of ABT took place predominantly at the grain edge of Au.

To understand the excitation mechanism in the photoisomerization, the electronic structure of ABT SAM on the Au surface and the density of states of the Au substrate should be taken into account. Tegeder and co-workers proposed a substrate-mediated charge transfer process for the photoisomerization of TBA on a Au surface.[7] UV light first generates hot holes in the Au d-band, which subsequently relax to the top of the d-band through an Auger decay. The hot holes undergo a charge transfer process to the HOMO of TBA, leading to the formation of transient positive ions, which may subsequently result in the isomerization of TBA. According to density functional theory (DFT) calculations (Supporting Information, Figure S15), the energy levels of the step edge Au atoms shift to higher values compared to those of Au atoms on the terrace because of unsaturation and a decrease in inter-atom coupling.[41] The higher the d-band center, the higher the reactivity.[42] Moreover, we calculated the total energy of *trans*-ABT isomers and *cis*-ABT isomers adsorbed on an Au terrace and a 2-atom step edge, respectively (see the Supporting Information, Figure S16). The reaction enthalpy of *trans*-to-*cis* isomerization at the 2-atom step edge is 0.61 eV, which is 13% lower than that at the terrace (0.72 eV). Therefore, the *cis* isomers of ABT on step edges are thermodynamically more stable compared to those on terrace sites. It is fairly well established, for example, that the *cis* isomers of TBI are preferentially found on the herringbone reconstruction of Au, as observed from STM images because of the slight corrugation at these sites.[18]

Moreover, because of the completely different geometry at grain edges, the molecular orientation of ABT molecules adsorbed at these sites is different from that of ABT molecules adsorbed at the terraces of Au, which could favor the *trans*-to-*cis* photoisomerization of ABT (Supporting Information, Figure S17).

In summary, a low-cost TS Au substrate with a number of steps was fabricated and used for the investigation of photoisomerization of an ABT SAM using STM-TERS. TER spectra of ABT SAM before and after UV light illumination were collected. Based on the presence of the υ_{sym}(N=N) peak at 1525 cm^{-1}, the *cis* isomer of azobenzene thiol could be clearly distinguished from the *trans* isomer. The *trans*/*cis* conformational change of ABT molecules after UV light illumination was monitored by TER imaging. Furthermore, we discovered that the photoisomerization yield of ABT molecules at Au grain edges is higher than that on Au terraces because the *cis*-to-*trans* back-reaction rate is slower at the grain edges of Au. This is ascribed to the shift of d-bands to higher energy and the lower reaction enthalpy of *trans*-to-*cis* isomerization at Au steps, as confirmed by DFT. These results confirm a substrate-mediated charge transfer process for the photoisomerization of ABT on a Au surface. The ability to spatially distinguish the molecular vibrational features of molecules adsorbed at different surface sites will contribute to a better understanding of the photoisomerization mechanism of photoswitches bound to a metal surface.

Acknowledgements

L.-Q.Z. thanks the Chinese Scholarship Council for a Ph.D. student fellowship. We thank the High Performance Computing Team at ETH Zurich for help with the DFT calculations, Dr. Ewelina Lipiec and Jacek Szczerbinski for helpful discussions, and Dr. Alessandro Lauria for help with recording UV/Vis spectra.

Conflict of interest

The authors declare no conflict of interest.

Keywords: azobenzene thiols · grain edges · photoisomerization · substrate-mediated charge transfer · tip-enhanced Raman spectroscopy

How to cite: *Angew. Chem. Int. Ed.* **2018**, *57*, 1025 – 1029
Angew. Chem. **2018**, *130*, 1037 – 1041

[1] H. Qian, S. Pramanik, I. Aprahamian, *J. Am. Chem. Soc.* **2017**, *139*, 9140 – 9143.
[2] Y. B. Zheng, B. Kiraly, S. Cheunkar, T. J. Huang, P. S. Weiss, *Nano Lett.* **2011**, *11*, 2061 – 2065.
[3] V. Balzani, A. Credi, F. M. Raymo, J. F. Stoddart, *Angew. Chem. Int. Ed.* **2000**, *39*, 3348 – 3391; *Angew. Chem.* **2000**, *112*, 3484 – 3530.
[4] J. Robertus, W. R. Browne, B. L. Feringa, *Chem. Soc. Rev.* **2010**, *39*, 354 – 378.
[5] N. Tamai, O. H. Miyasaka, *Chem. Rev.* **2000**, *100*, 1875 – 1890.
[6] H. M. D. Bandara, S. C. Burdette, *Chem. Soc. Rev.* **2012**, *41*, 1809 – 1825.
[7] M. Wolf, P. Tegeder, *Surf. Sci.* **2009**, *603*, 1506 – 1517.
[8] J. Plain, G. P. Wiederrecht, S. K. Gray, P. Royer, R. Bachelot, *J. Phys. Chem. Lett.* **2013**, *4*, 2124 – 2132.
[9] Z. Mahimwalla, K. G. Yager, J. I. Mamiya, A. Shishido, A. Priimagi, C. Barrett, *J. Polym. Bull.* **2012**, *69*, 967 – 1006.
[10] T. J. Kucharski, N. Ferralis, A. M. Kolpak, J. O. Zheng, D. G. Nocera, J. C. Grossman, *Nat. Chem.* **2014**, *6*, 441 – 447.
[11] Y. Wang, N. Ma, Z. Wang, X. Zhang, *Angew. Chem. Int. Ed.* **2007**, *46*, 2823 – 2826; *Angew. Chem.* **2007**, *119*, 2881 – 2884.
[12] Y. B. Zheng, J. L. Payton, P. S. Weiss, et al., *Nano Lett.* **2011**, *11*, 3447 – 3452.
[13] H. Rau, E. Lueddecke, *J. Am. Chem. Soc.* **1982**, *104*, 1616 – 1620.
[14] R. Turanský, M. Konôpka, N. L. Doltsinis, I. Stich, D. Marx, *Phys. Chem. Chem. Phys.* **2010**, *12*, 13922 – 13932.
[15] G. S. Hartley, *J. Chem. Soc.* **1938**, 633 – 642.
[16] J. Henzl, M. Mehlhorn, H. Gawronski, K. H. Rieder, K. Morgenstern, *Angew. Chem. Int. Ed.* **2006**, *45*, 603 – 606; *Angew. Chem.* **2006**, *118*, 617 – 621.
[17] R. Schmidt, S. Hagen, D. Brete, R. Carley, C. Gahl, J. Dokc, P. Saalfrank, S. Hecht, P. Tegeder, M. Weinelt, *Phys. Chem. Chem. Phys.* **2010**, *12*, 4488 – 4497.
[18] C. Gahl, D. Brete, F. Leyssner, M. Koch, E. R. McNellis, J. Mielke, R. Carley, L. Grill, K. Reuter, P. Tegeder, M. Weinelt, *J. Am. Chem. Soc.* **2013**, *135*, 4273 – 4281.
[19] N. Tallarida, L. Rios, V. A. Apkarian, J. Lee, *Nano Lett.* **2015**, *15*, 6386 – 6394.
[20] Y. Ootani, K. Satoh, A. Nakayama, T. Noro, T. Taketsugu, *J. Chem. Phys.* **2009**, *131*, 194306.
[21] M. Pederzoli, J. Pittner, M. Barbatti, H. Lischka, *J. Phys. Chem. A* **2011**, *115*, 11136 – 11143.
[22] V. Cantatore, G. Granucci, M. Persico, *Comput. Theor. Chem.* **2014**, *1040 – 1041*, 126 – 135.
[23] D. P. Hoffman, S. R. Ellis, R. A. Mathies, *J. Phys. Chem. A* **2013**, *117*, 11472 – 11478.
[24] M. Quick, A. L. Dobryakov, M. Gerecke, C. Richter, F. Berndt, I. N. Ioffe, A. A. Granovsky, R. Mahrwald, N. P. Ernsting, S. A. Kovalenko, *J. Phys. Chem. B* **2014**, *118*, 8756 – 8771.
[25] A. L. Dobryakov, M. Quick, I. N. Ioffe, A. A. Granovsky, N. P. Ernsting, S. A. Kovalenko, *J. Chem. Phys.* **2014**, *140*, 184310.
[26] M. Alemani, S. Selvanathan, F. Ample, M. V. Peters, K. H. Rieder, F. Moresco, C. Joachim, S. Hecht, L. Grill, *J. Phys. Chem. C* **2008**, *112*, 10509 – 10514.
[27] X. Wang, S.-C. Huang, T.-X. Huang, H.-S. Su, J.-H. Zhong, Z.-C. Zeng, M.-H. Li, B. Ren, *Chem. Soc. Rev.* **2017**, *46*, 4020 – 4041.
[28] T. Schmid, L. Opilik, C. Blum, R. Zenobi, *Angew. Chem. Int. Ed.* **2013**, *52*, 5940 – 5954; *Angew. Chem.* **2013**, *125*, 6054 – 6070.
[29] G. Ertl, *Angew. Chem. Int. Ed.* **2013**, *52*, 52 – 60; *Angew. Chem.* **2013**, *125*, 52 – 61.
[30] R. M. Stöckle, Y. D. Suh, V. Deckert, R. Zenobi, *Chem. Phys. Lett.* **2000**, *318*, 131 – 136.
[31] M. S. Anderson, *Appl. Phys. Lett.* **2000**, *76*, 3130 – 3132.
[32] N. Hayazawa, Y. Inouye, Z. Sekkat, S. Kawata, *Opt. Commun.* **2000**, *183*, 333 – 336.
[33] B. Pettinger, P. Schambach, C. J. Villagómez, N. Scott, *Annu. Rev. Phys. Chem.* **2012**, *63*, 379 – 399.
[34] H. K. Wickramasinghe, M. Chaigneau, R. Yasukuni, G. Picardi, R. Ossikovski, *ACS Nano* **2014**, *8*, 3421 – 3426.
[35] R. Zhang, Y. Zhang, Z. C. Dong, S. Jiang, C. Zhang, L. G. Chen, L. Zhang, Y. Liao, J. Aizpurua, Y. Luo, J. L. Yang, J. G. Hou, *Nature* **2013**, *498*, 82 – 86.
[36] J.-H. Zhong, X. Jin, L. Meng, X. Wang, H.-S. Su, Z.-L. Yang, C. T. Williams, B. Ren, *Nat. Nanotechnol.* **2017**, *12*, 132 – 136.
[37] G. Pace, V. Ferri, C. Grave, M. Elbing, C. V. Hänisch, M. Zharnikov, M. Mayor, M. A. Rampi, P. Samori, *Proc. Natl. Acad. Sci. USA* **2007**, *104*, 9937 – 9942.
[38] M. Hegner, P. Wagner, G. Semenza, *Surf. Sci.* **1993**, *291*, 39 – 46.
[39] J. P. Merrick, D. Moran, L. Radom, *J. Phys. Chem. A* **2007**, *111*, 11683 – 11700.
[40] C. M. Stuart, R. R. Frontiera, R. A. Mathies, *J. Phys. Chem. A* **2007**, *111*, 12072 – 12080.
[41] B. Hammer, J. K. Nørskov, *Adv. Catal.* **2000**, *45*, 71 – 129.
[42] Z.-P. Liu, P. Hu, *J. Am. Chem. Soc.* **2002**, *124*, 14770 – 14779.

Manuscript received: October 10, 2017
Revised manuscript received: November 25, 2017
Accepted manuscript online: November 27, 2017
Version of record online: December 27, 2017

Angewandte Chemie
Eine Zeitschrift der Gesellschaft Deutscher Chemiker

Supporting Information

Nanoscale Chemical Imaging of Reversible Photoisomerization of an Azobenzene-Thiol Self-Assembled Monolayer by Tip-Enhanced Raman Spectroscopy

*Li-Qing Zheng, Xing Wang, Feng Shao, Martin Hegner, and Renato Zenobi**

anie_201710443_sm_miscellaneous_information.pdf

Experimental Section

A freshly stripped Au substrate [1] was immersed in a 1 mM ABT (ProChimia Surfaces, Poland) solution dissolved in ethanol for 2 h to allow the formation of a SAM on the surface. After immersion, the sample was rinsed with ethanol and dried under an N_2 atmosphere. After UV irradiation for different time, the sample was directly used for STM and TERS measurement. Four 5 W UV LED lamps with a wavelength of 365 nm were used as light source. The distance between light source and the sample was kept at 5 mm, which resulted in a light intensity of 160 mW/cm^{-2}. The 5W blue LED lamps with the wavelength of 450 nm were used as another light source.

AFM and STM measurements were performed on instruments from NT-MDT (Zelenograd, Russia). Aspire CT300R-25 silicon tips (Nanoscience instruments, USA) with a resonance frequency of 300 kHz and a spring constant of 42 N/m (tapping mode) were used for AFM imaging. An electrochemically etched Ag tip [2] was used for STM imaging.

STM-TERS measurements was performed on a top illumination TERS instrument that combines STM with a Raman spectrometer (NT-MDT, Russia, NTEGRA Spectra Upright). An electrochemically etched Ag tip was used to obtain both the topography and TER spectra. The 632.8 nm He-Ne laser was used as an excitation source. For all the measurements, the tunneling conditions were 200 pA and 0.2 V, the intensity of laser was 68 μW with 1s exposure time.

UV-Vis spectra of ABT in ethanol solution were recorded by a GENESYS 10S UV-Vis spectrophotometer (Thermo Scientific, USA). UV-Vis spectra of an ABT SAM on an Au substrate were recorded by a V660 UV-Vis spectrophotometer (Brechbühler AG, Switzerland). The sample was prepared with the following method: An Au film with a thickness of 10 nm was prepared on quartz by thermal evaporation under high vacuum. The UV-Vis spectrum of this Au substrate was collected first, and then this Au substrate was

immersed in ABT ethanolic solution for 2 h to obtain the ABT SAM on the Au substrate. After immersion, the sample was rinsed by ethanol and dried under N_2 atmosphere. The UV-Vis spectrum of this ABT SAM on the Au substrate was then collected. The irradiation of the ABT SAM was performed in situ inside the spectrometer.

Supporting figures

200 nm Au evaporated onto a mica substrate at 300 ^{o}C under high vacuum were fabricated in 1993, and we glued them to Si wafers with epoxy glue. [1] After chemically stripping with THF, a clean Au surface was obtained and used as a substrate for our experiments (Figure S1). The STM image showed a number of steps (Figure S1B), which renders this substrate very suitable for studying surface reactions at different surface sites. Compared with other results shown in the literature [1], the quality of this Au substrate, which was fabricated in 1993, had not changed with time, suggesting that such Au-mica bilayers have excellent long-term stability.

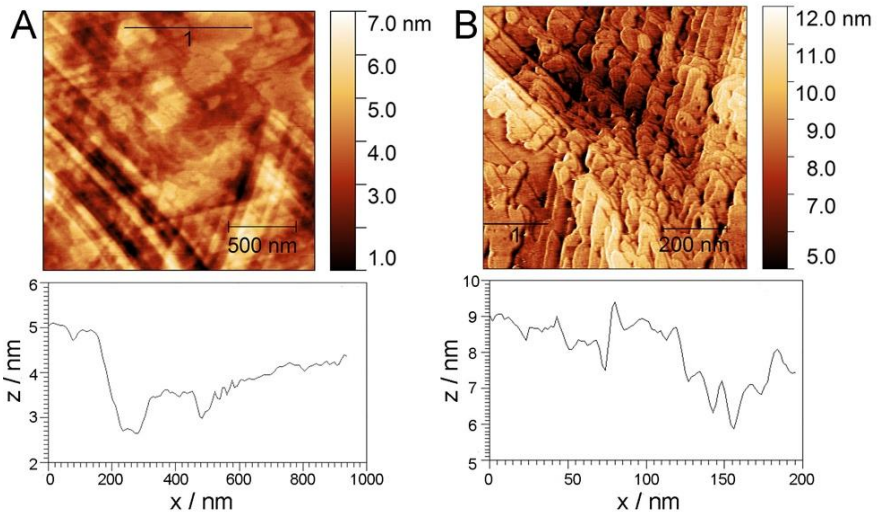

Figure S1. A. AFM image of a TS Au surface fabricated 24 years ago. The scan area is 2 µm x 2 µm. B. STM image of the same substrate on a scale of 800 nm. Insets below the images are height profiles along the lines indicated in the images. The tunneling conditions were 200 pA and 0.2 V.

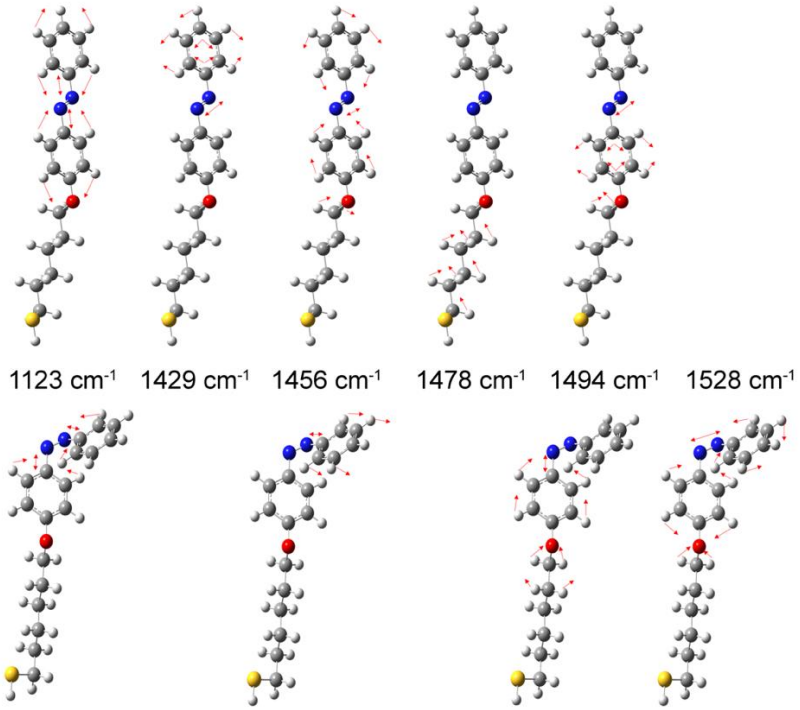

Figure S2. Schematic of different modes for trans and cis isomers.

Table S1. Different peak intensity ratios of the TER spectra of an ABT SAM before and after UV irradiation for 5 mins (shown in Figure 1A)

Peak intensity ratio	Before UV irradiation	After UV irradiation
1145 cm^{-1} / 1600 cm^{-1}	4.98	3.62
1186 cm^{-1} / 1600 cm^{-1}	2.07	1.89
1418 cm^{-1} / 1600 cm^{-1}	2.52	2.20
1447 cm^{-1} / 1600 cm^{-1}	3.05	2.69
1469 cm^{-1} / 1600 cm^{-1}	2.73	2.26

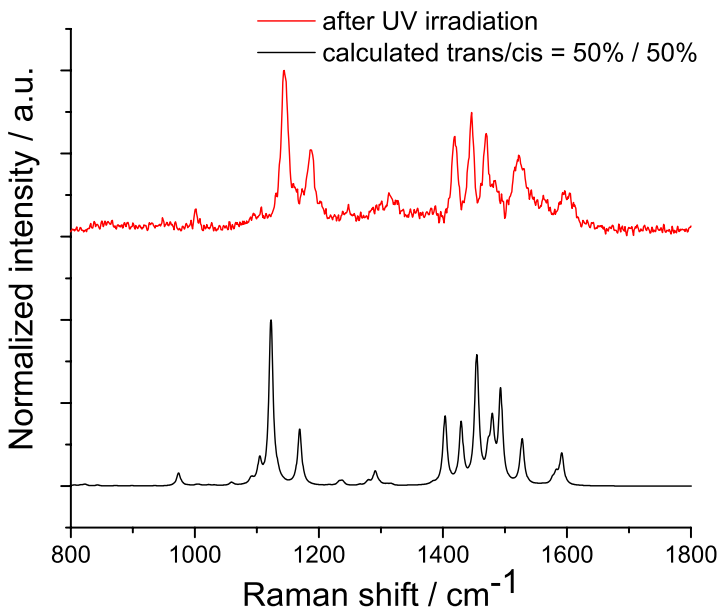

Figure S3. TER spectrum of ABT SAM after UV irradiation for 5 mins (red) and simulated Raman spectrum of trans and cis isomers in a 50% / 50% molar ratio (black).

Table S2. Absorbance difference at 340 nm of an ABT SAM on an Au substrate upon irradiation of UV light and blue light

Samples	**Δ Absorbance at 340 nm**
ABT SAM	0
ABT SAM after UV irradiation for 5 mins	$- 3.4 \times 10^{-3}$
ABT SAM after UV irradiation for 15 mins	$- 3.4 \times 10^{-3}$
ABT SAM after UV irradiation for 15 mins and then blue light irradiation for 15 mins	$- 1.2 \times 10^{-3}$

Δ Absorbance values shown in the table were obtained by subtracting the absorbance at 340 nm of the ABT SAM before UV irradiation.

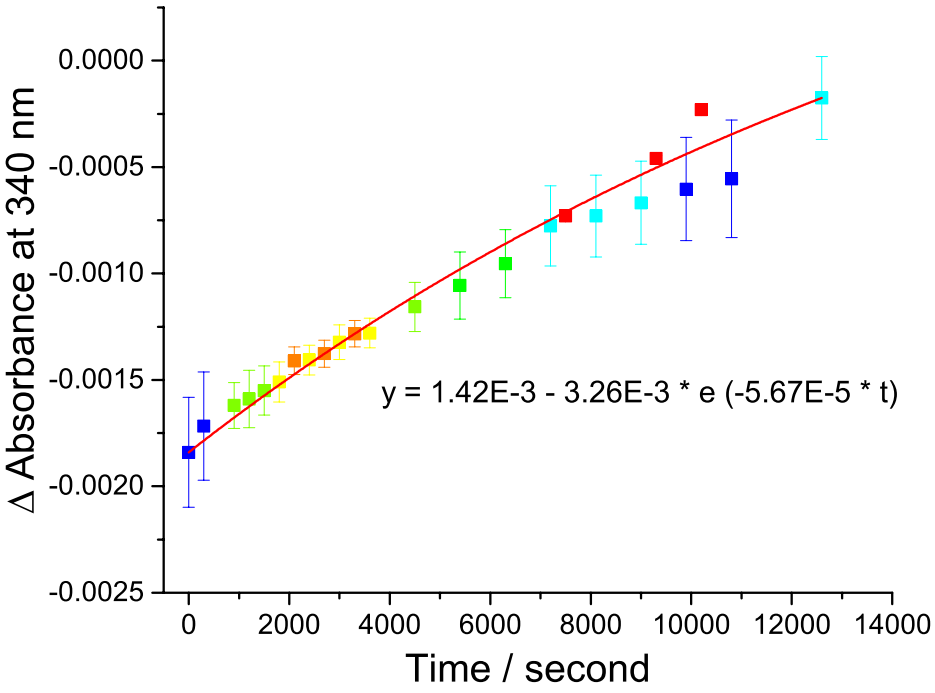

Figure S4. Absorbance difference at 340 nm of an ABT SAM on an Au surface after UV irradiation for 5 mins as a function of time. The absorbance differences shown were obtained by subtracting the absorbance at 340 nm of the ABT SAM before UV irradiation. The red, orange and yellow data points have smaller error bars than the green, light blue and dark blue data points. The red line represents a first-order kinetic fit of the experimental data, with $k = 5.67 \times 10^{-5}$ s^{-1}.

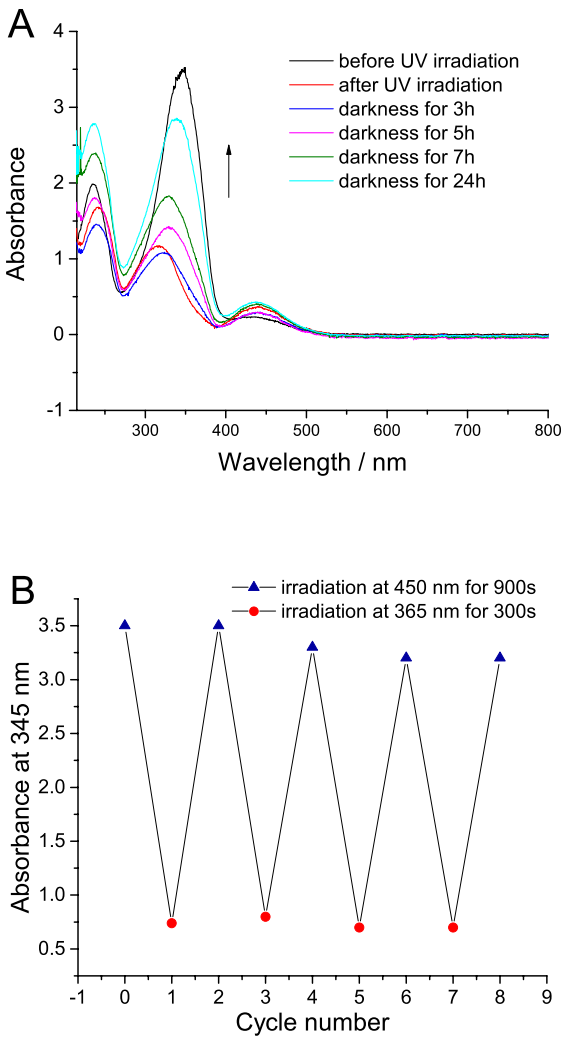

Figure S5. A. UV-Vis spectra of ABT in ethanol solution before and after UV irradiation for 5 mins, and then the solution was kept in the dark for different time; B. Changes of the absorbance at 345 nm of ABT in ethanol solution (c = 0.2 mM) upon alternating irradiation with UV and blue light.

To compare the different isomerization rates of ABT on a solid surface and in a solution, UV-Vis spectra of ABT in ethanol solution (concentration = 0.2 mM) before and after UV irradiation for 5 mins were collected. As shown in Figure S5A, upon UV irradiation for 5 mins, the π–π* absorption peak at 345 nm corresponding to the trans isomer decreases, while

the n–π* absorption peak at 430 nm of the cis isomer increases, indicating trans-to-cis photoisomerization. The absorption peak intensity of the cis ABT isomer was divided by that of the cis isomer to calculate the molar ratio between the two isomers. The cis-to-trans molar ratio is > 30 % after UV irradiation for 5 mins. The sample was kept in the dark for different times after UV irradiation. The molar ratio of cis isomers decreased to 15% after storage for 24 h due to the thermal back reaction. On alternating irradiation with UV and blue light, this reversible photoisomerization process can be recycled many times (see Figure S5B). After the second cycle, we see a slight decrease in the absorption at 345 nm which could be attributed to slight photodegradation of ABT molecules.

Section S3: Principal component analysis (PCA)

To assess the variability of the peak at 1525 cm^{-1} associated with the isomerization of ABT, a principal component analysis (PCA) was used to analyze the TERS map of Figure 2B. The loading plots of different PCs and the corresponding PC score maps are shown in Figure S6. We can see that the baseline of the loading plots is not flat, which is due to the different enhancement activity of a tip at different surface area. To gain further insight, the loading plot of PC1versus PC2 is shown in Figure. S7. PC1 contributed 58 % of the total variance, while PC2 contributed 16% of the total variance. In PC1, all the positive and negative loadings are attributed to the Raman peaks of the trans isomer. Other than the trans Raman peaks, positive loadings at 1106 cm^{-1} and 1525 cm^{-1} correspond to the C-N stretching mode and the N=N stretching mode of the cis isomer are shown in PC2, which indicates that PC2 may be a convoluted Raman spectrum of the trans and cis isomers. The differences between PC1 and PC2 are quite small, which could be ascribed to the 10 times intensity drop of ABT cis isomers. Finally, PC3 makes up 4% of the total variance. In PC3, the strong positive

loading at 1280, 1350 cm^{-1} and negative loading at 1550 cm^{-1} are related to carbonaceous decomposition products. This suggests that sample decomposition is minor.

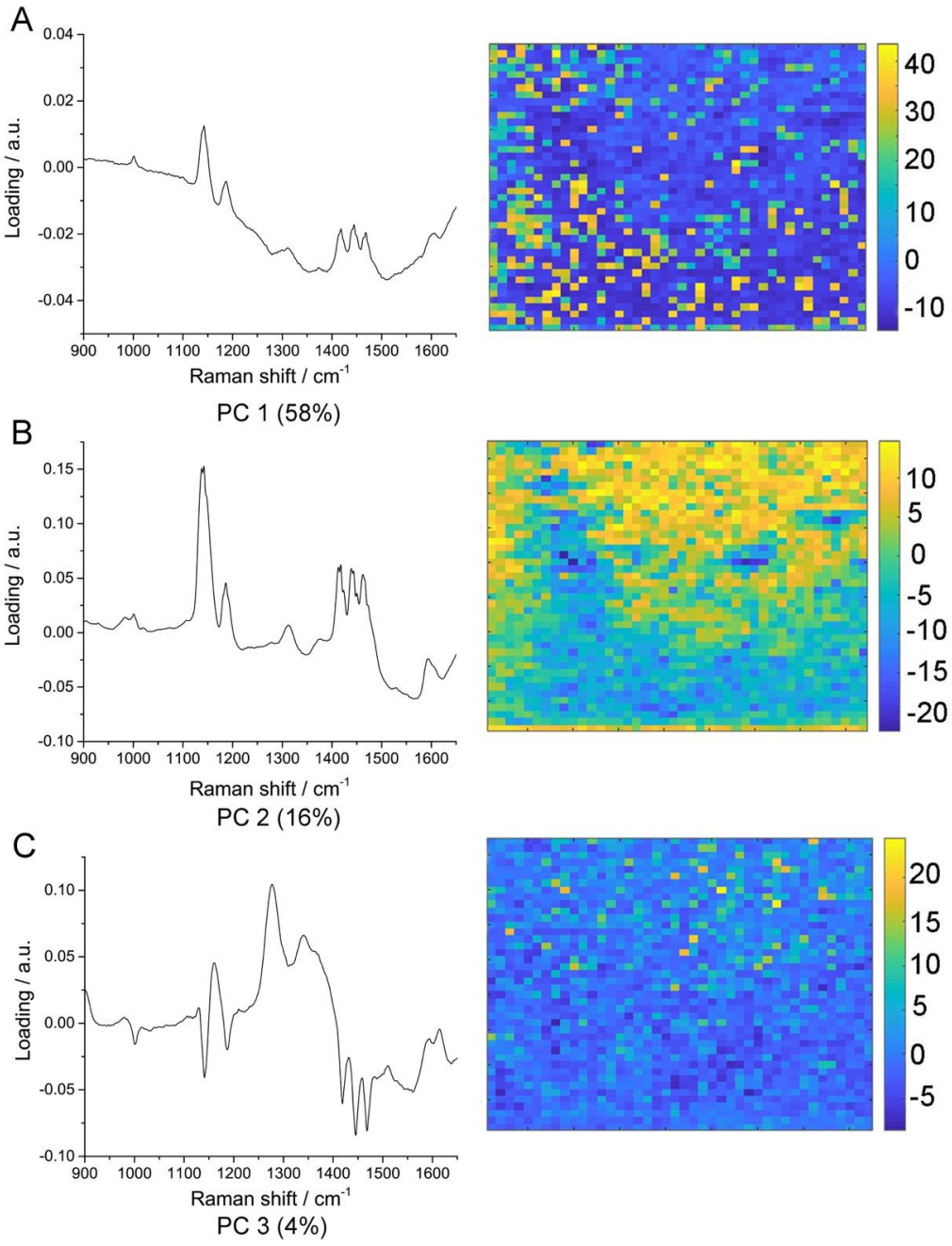

Figure S6. Loading plots of TER spectra collected in the TERS map of Figure 2B and corresponding score maps.

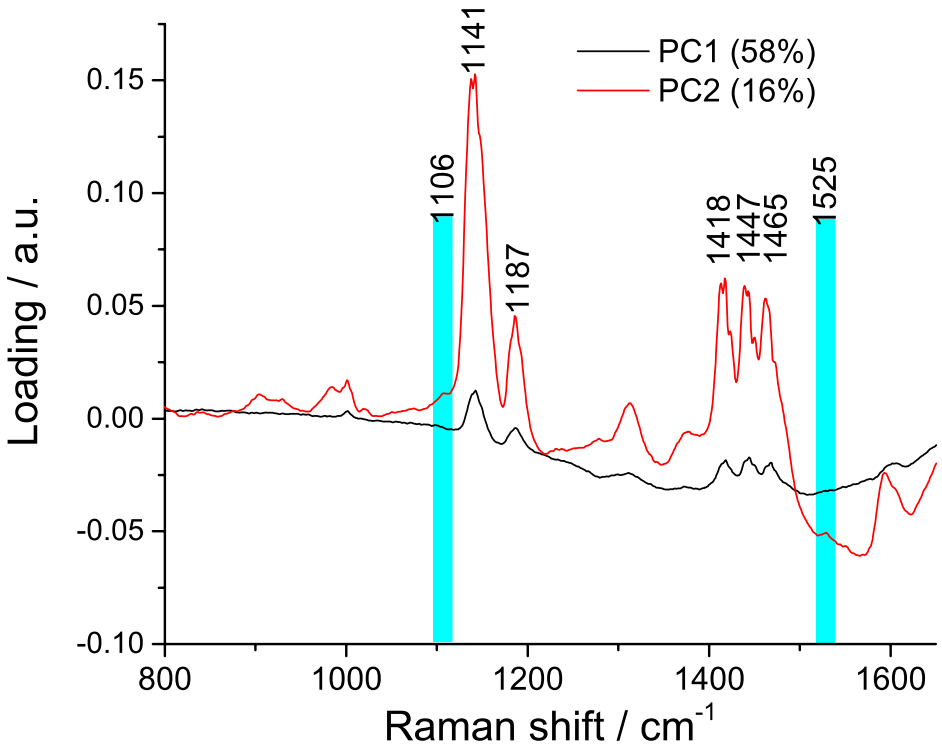

Figure S7. Loading plots of PC1 and PC2

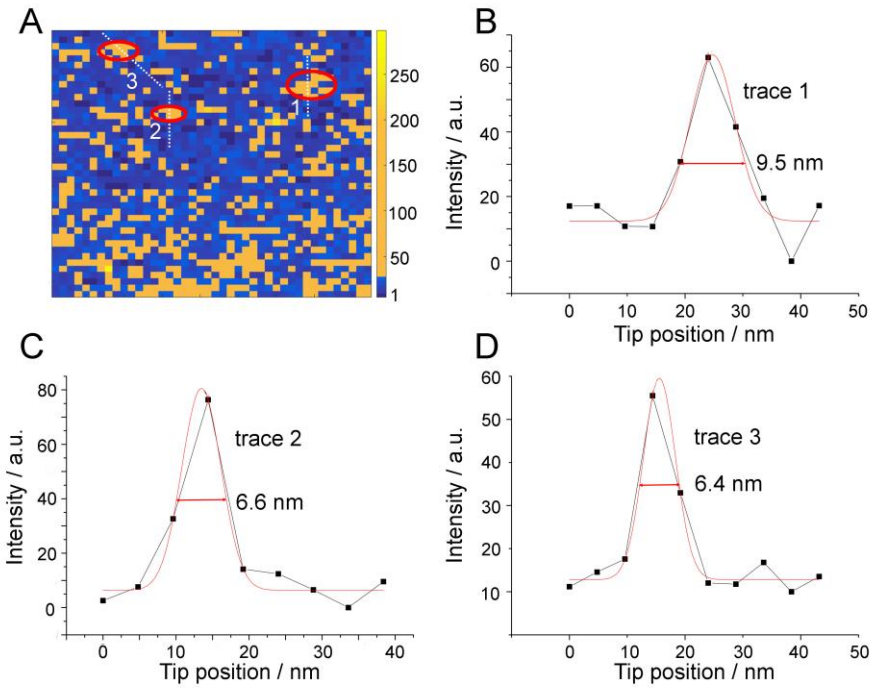

Figure S8. A. TERS map of the Raman peak intensity at 1525 cm^{-1} of ABT SAM after UV irradiation for 15 mins. The size of the maps is 200 x 200 nm^2 with 4.8 nm pixel size. The tunneling conditions were 200 pA and 0.2 V. The intensity of red laser (632 nm) was 68 μW with 1s exposure time. Plots of TERS intensities at 1525 cm^{-1} with the tip position along the trace 1 (B), trace 2 (C) and trace 3 (D) indicated in Fig. 4A.

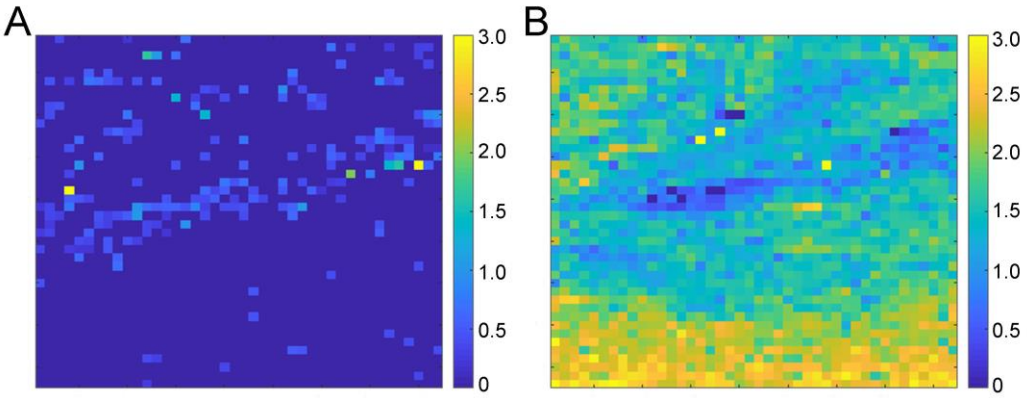

Figure S9. A. TERS peak intensity ratio (1525 cm^{-1} peak / 1600 cm^{-1} peak) map of an ABT SAM after UV irradiation for 5 mins followed by blue light irradiation for 5 mins; B. TERS peak intensity ratio (1418 cm^{-1} peak / 1600 cm^{-1} peak) map of an ABT SAM after UV irradiation for 5 mins followed by blue light irradiation for 5 mins.

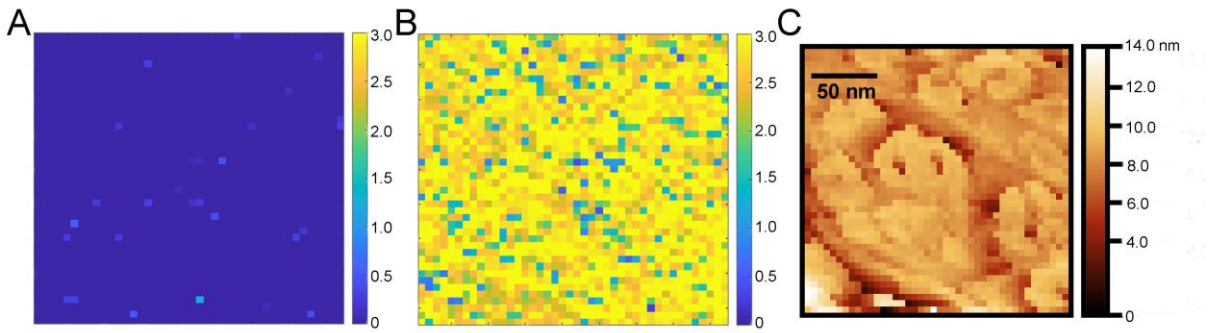

Figure S10. A. TERS peak intensity ratio (1525 cm^{-1} peak / 1600 cm^{-1} peak) map of an ABT SAM before UV irradiation; B. TERS peak intensity ratio (1418 cm^{-1} peak / 1600 cm^{-1} peak) map of an ABT SAM before UV irradiation. C. STM image of ABT SAM on the Au surface acquired together with the TERS map. The size of the map is 200 x 200 nm^2, with a 4.8 nm pixel size. The acquisition time for each spectrum was 1s.

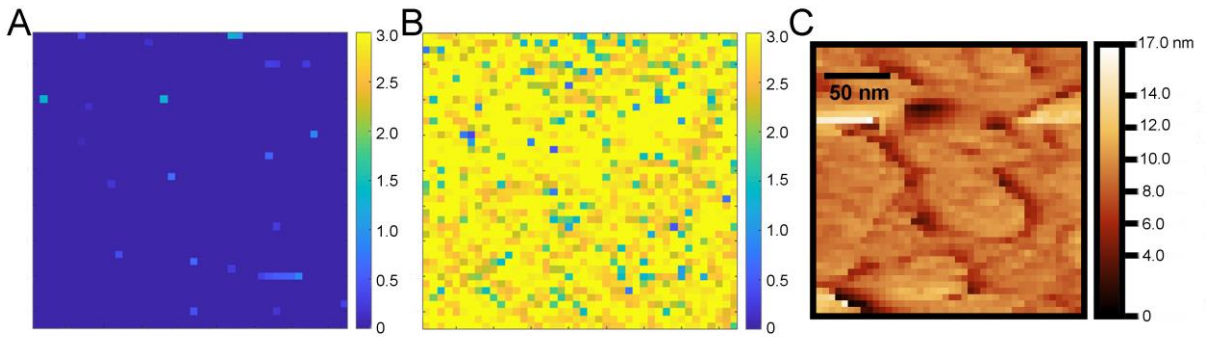

Figure S11. A. TERS peak intensity ratio (1525 cm^{-1} peak / 1600 cm^{-1} peak) map of an ABT SAM before UV irradiation; B. TERS peak intensity ratio (1418 cm^{-1} peak / 1600 cm^{-1} peak) map of an ABT SAM before UV irradiation. C. STM image of ABT SAM on the Au surface acquired together with the TERS map. The size of the map is 200 x 200 nm^2, with a 4.8 nm pixel size. The acquisition time for each spectrum was 1s.

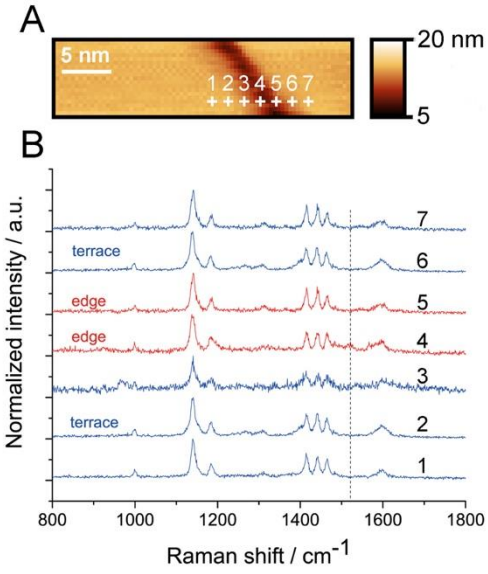

Figure S12. A. STM image of the Au surface with ABT SAM, obtained using a Ag tip; B. line-trace TER spectra along the crosses indicated in A. The tunneling conditions were 200 pA and 0.2 V. The intensity of red laser (632 nm) was 68 μW with 1s exposure time. One spectrum was acquired every 2 nm of surface distance.

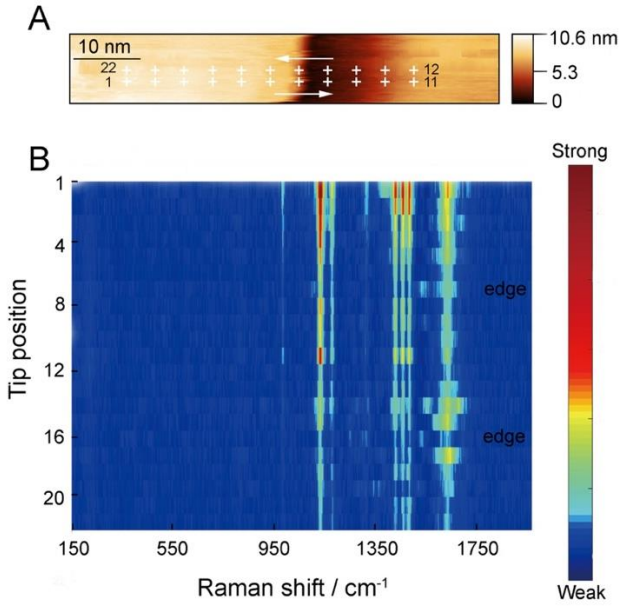

Figure S13. A. STM image of the Au surface with ABT SAM, obtained using a Ag tip; B. line-trace and line-retrace TER spectra along the crosses indicated in A. The tunneling conditions were 200 pA and 0.2 V. The intensity of red laser (632 nm) was 68 μW with 1s exposure time. One spectrum was acquired every 4 nm of surface distance.

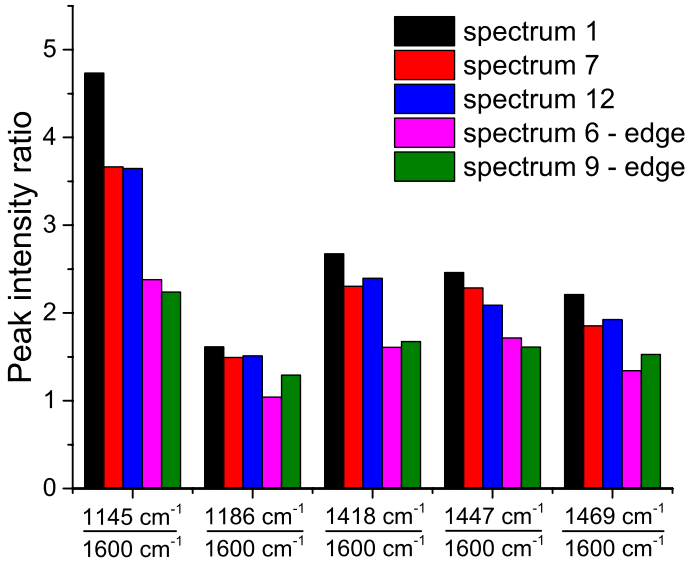

Figure S14. Peak intensity ratios in the TER spectra of ABT adsorbed at different surface sites after UV irradiation (shown in Figure 4B). The spectra 1, 7 and 12 correspond to the TER spectra of ABT adsorbed on the Au terraces; The spectra 6 and 9 correspond to the TER spectra of ABT adsorbed on the grain edge of Au.

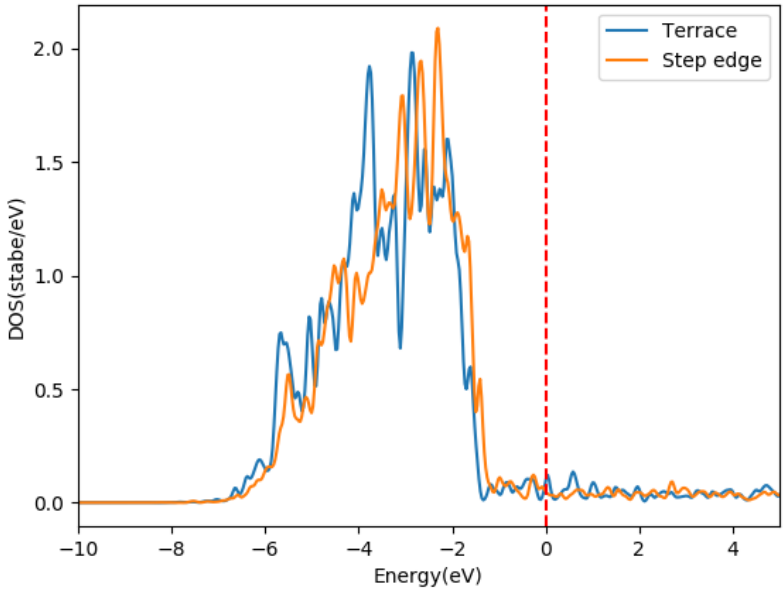

Figure S15. Calculated projected electronic density of state (DOS) of Au atoms at different surface sites.

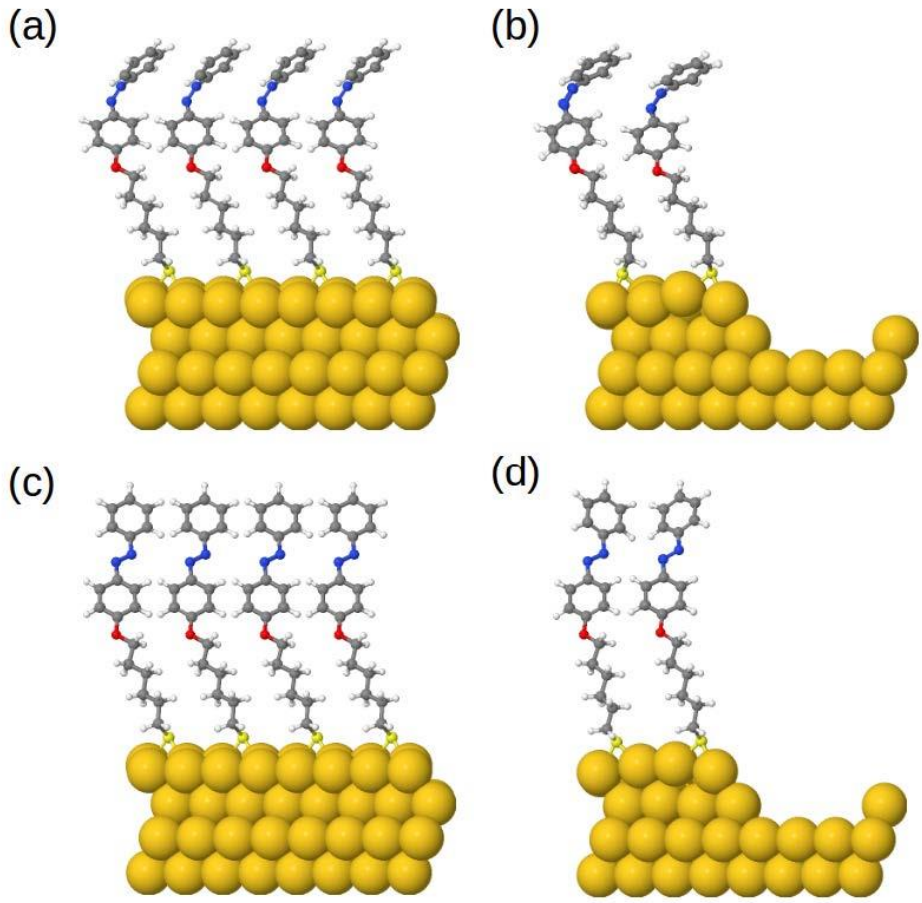

Figure S16. Terrace and step models after DFT calculation. A. ABT cis isomers adsorbed on a Au terrace; B. ABT cis isomers adsorbed on a Au step; C. ABT trans isomers adsorbed on a Au terrace; D. ABT cis isomers adsorbed on a Au step.

Computational models and methods

The Quickstep module in the CP2K simulation package was employed for DFT calculations [3]. The generalized gradient approximation (GGA) using the Perdew, Burke and Ernzerhof (PBE) functional was used to describe the exchange-correlation energy [4]. The double-zeta valence plus polarization (DZVP) basis set and Geodecker-Teter-Hutter (GTH) potentials [5] with 11, 1, 4, 6, 5 and 6 valence electrons for Au, H, C, O, N and S atom were used for the calculations. A cutoff of 500 Ry was used for the auxiliary plane wave expansion

of the charge density. The Au substrate is modeled by a p (4×8) cell of Au (111) surface. The bottom two atomic layers of Au are kept frozen and set to the bulk parameters, while the remaining layers are fully relaxed during the calculations. A vacuum region of thickness higher than 15 Å was used to guarantee no interactions between the slabs.

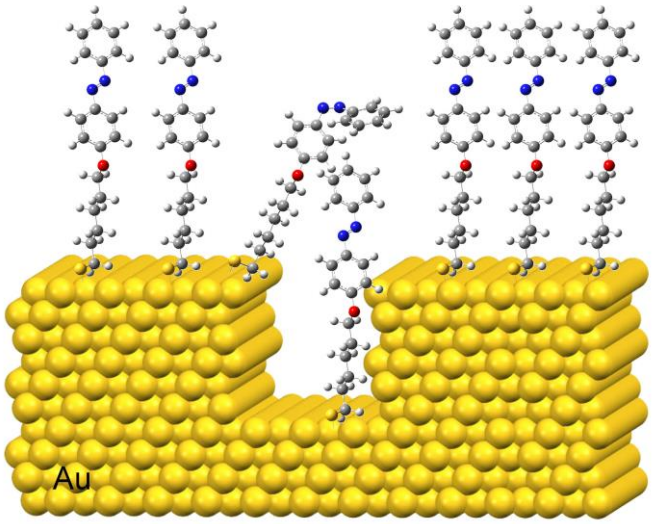

Figure S17. Schematic of the trans-to-cis photoisomerization of an ABT molecule adsorbed at the edge of a Au grain.

References

[1] M. Hegner, P.Wagner and G. Semenza, *Surf. Sci.*, **1993**, 291, 39-46.

[2] J. Stadler, T. Schmid, R. Zenobi, Nano Lett., **2010**, 10, 4514-4520.

[3] J. VandeVondele, M. Krack, F. Mohamed, M. Parrinello, T. Chassaing and J. Hutter, Comput. Phys. Commun., **2005**, 167, 103-128.

[4] J. P. Perdew, K. Burke and M. Ernzerhof, Phys. Rev. Lett., **1996**, 77, 3865-3868.

[5] S. Goedecker, M. Teter and J. Hutter, Phys. Rev. B, **1996**, 54, 1703-1710.